Int J CARS (2009) 4:579–587
DOI 10.1007/s11548-009-0373-3

ORIGINAL ARTICLE

An improved finite element model for craniofacial surgery simulation

Shengzheng Wang · Jie Yang

Received: 5 January 2009 / Accepted: 22 May 2009 / Published online: 13 June 2009

Abstract
Purpose A novel approach is proposed for simulating the deformation of the facial soft tissues in the craniofacial surgery simulation.
Methods A nonlinear finite mixed-element model (NFM-EM) based on solid-shell elements and Lagrange principle of virtual work is proposed, which addresses the heterogeneity in geometry and material properties found in the soft tissues of the face. Moreover, after the investigation of the strain-potential models, the biomechanical characteristics of skin, muscles and fat are modeled with the most suitable material properties. In addition, an improved contact algorithm is used to compute the boundary conditions of the soft tissue model.
Results The quantitative validation and the comparative results with other models proved the effectiveness of the approach on the simulation of complex soft tissues. The average absolute value of errors stays below 0.5 mm and the 95% percentiles of the distance map is less than 1.5 mm.
Conclusions NFM-EM promotes the accuracy and effectiveness of the soft tissue deformation, and the effective contact algorithm bridges the bone-related planning and the prediction of the target face.

Keywords Nonlinear finite mixed-element modeling · Contact algorithm · Soft tissue deformation · Craniofacial surgery

Introduction

Cranio-maxillofacial surgery is to restore the patient's normal face through repositioning of bones or cranioplasty and thus in the computer-assisted surgical (CAS) planning system, the capacity to predict the realistic motion of the facial tissues is a huge demand for surgeons [1]. Therefore, the prediction of the soft tissue deformation becomes highly desirable in the surgical planning system. During the past decade, many research efforts have been dedicated to simulating the behaviors of the soft tissue deformation. In the beginning, many research works were mainly focused on facial animation based on masses and springs [2,3], which inspired the development of the cranio-maxillofacial soft tissue prediction systems. Subsequently, some anatomy-based facial tissue models were proposed using finite element method [4,5]. Furthermore, the real-time simulation using elastic finite element was implemented in [6–9], and an early survey about real-time soft tissue simulation can be found in [10]. These methods obtained realistic visual results. However, the biomechanical characteristics of the facial tissues were not incorporated into their models, which affected the effectiveness of the soft tissue deformation. Many other researchers followed up to put emphasis on biomechanical models of the soft tissue deformation [11–16]. Two years later, some researchers validated the effectiveness of the biomechanical models to boost the clinic practice of the CAS planning system [1,17,18]. During the simulation, however, too much prior assumption and knowledge were required. Moreover, these methods cannot model the accurate physical behaviors in such complex parts of the face as mid-face, mandible and so on.

These drawbacks of previous methods result from at least three aspects. (1) The soft tissues of the face were modeled with homogenous materials, without distinguishing among skin, muscles and fat, which resulted in lacking accuracy of the soft tissue deformation. (2) The geometric models of the soft tissues of the face were built using a unified mesh type based on either surface element or solid element. But since

S. Wang (✉) · J. Yang
Shanghai Jiao Tong University, Shanghai, China
e-mail: szwang.smu@gmail.com

the skin and muscles have very different geometric structures, they cannot be easily modeled using the unified mesh type. (3) In conventional methods, the boundary conditions of the soft tissue model were defined by manual measurement or registration etc. It was assumed that the motion of a soft tissue point that adjoins to the bones equals the motion of that part of the bones.

The methodology presented in this paper has been defined to overcome some of the shortcomings of previous models. The new features of our approach are: (1) the skin and the internal tissues (muscles and fat) are modeled using different nonlinear biomechanical properties, (2) the nonlinear finite element modeling of the soft tissues is based on mixed elements so that the skin and the internal tissues are discretized into different mesh types, which improves the accuracy of the biomechanical model, and (3) the boundary conditions of the soft tissue model are computed dynamically based on bone-related planning.

The rest of the paper is organized as follows. "Method" section presents the new biomechanical model including the choice of materials, the mixed element modeling and the boundary condition computation. "Results" section shows the system implementation and preliminary results of the method and discusses the validation of our algorithm.

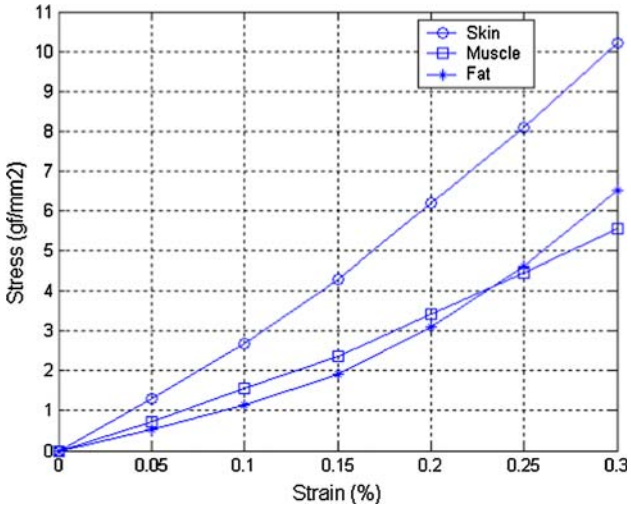

Fig. 1 The strain–stress relationship of the soft tissues

Table 1 Hyperelastic material parameters of the soft tissues for Mooney–Rivlin model (gf/mm^2)

Type	D_1	C_{10}	C_{01}
Skin	0.49	18.9834587	−15.4071649
Muscle	0.3	9.84540206	−7.74326281
Fat	0.49	16.6131140	−16.0126823

Method

Choice of materials

In this paper, the isotropic Mooney–Rivlin (M–R) [19] strain–energy potential model was used to simulate material properties of the soft tissues of the face.We assumed the soft tissue to be incompressible, homogeneous, and isotropic elastic material. The two-term Mooney–Rivlin equation is employed to represent the strain energy function and defined as

$$\bar{W}(I_1, I_2, I_3) = C_{10}(I_1 - 3) + C_{01}(I_2 - 3) \tag{1}$$

where C_{10} and C_{01} are material constants, and invariants of $\mathbf{C}$(the right Cauchy–Green tensor) are defined as: $I_1 = tr(\mathbf{C}) = \lambda_1^2 + \lambda_2^2 + \lambda_3^2$, $I_2 = \frac{1}{2}[(tr\mathbf{C})^2 - tr(\mathbf{C}^2)] = \lambda_1^2\lambda_2^2 + \lambda_2^2\lambda_3^2 + \lambda_3^2\lambda_1^2$,and $I_3 = \det(\mathbf{C}) = \lambda_1^2\lambda_2^2\lambda_3^2$, λ_i are the principal stretches.

For the soft tissues of the face, the coarse stress–strain relationship of the skin, muscles and fat is found in [20,21] and shown in Fig. 1. The material parameters used for the definition of the hyper-elastic model associated with the nonlinear mechanical definition of the soft tissues were estimated using ABAQUS 6.5 tools and presented in Table 1.

Therefore, the second Piola–Kirchhoff stress $\mathbf{S}$ can be derived from the right Cauchy–Green deformation tensor and the strain energy function

$$\mathbf{S} = 2\frac{\partial \bar{\mathbf{W}}}{\partial \mathbf{C}}. \tag{2}$$

By (1) and (2), the second Piola–Kirchhoff stress is obtained as

$$\mathbf{S} = 2C_{01}\mathbf{I} + 4C_{10}\mathbf{C} - (2C_{01} + 4C_{10})\mathbf{C}^{-1} \tag{3}$$

Mixed element modeling

The skin and muscles cannot be easily modeled using the same mesh type because they have the different geometric structures and different material properties (see Fig. 1). In order to better model the skin tissues and the internal tissues (muscles and fat), the skin tissues are discretized into triangular shell elements and the internal tissues into tetrahedral solid elements, as shown in Fig. 2. During the geometric model generation, the skin and skull surfaces are extracted with marching cubes algorithm [22] from CT data sets and optimized with mesh algorithms [23,24]. Then, the external surface of the internal tissues is obtained by moving the vertices of the skin surface along the vertex normal by an amount of ζ in negative direction, the assumed thickness of the skin. Generally, ζ averages 1.5 mm. At the same time, the tetrahedral solid elements of the internal tissues can be generated in terms of the external surface of the internal tissues, and

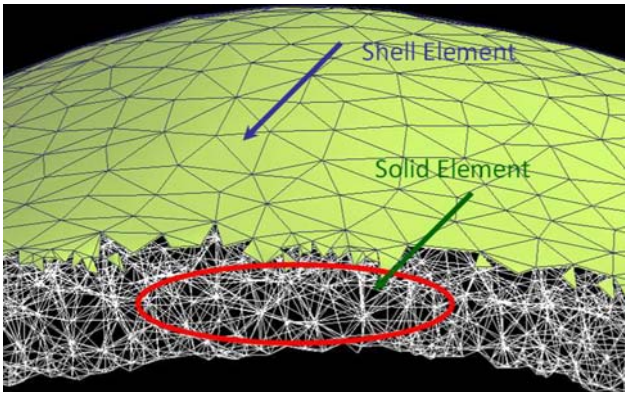

Fig. 2 The geometric model with solid-shell elements

the surface generated by moving the vertices along the vertex normal by an amount of 0.75 mm in negative direction is the mid-face of the shell elements.

However, additional problems arise when the shell elements are used in combination with the solid elements. The solid elements and the thin-shell elements cannot be connected due to the discontinuity of the rotation degrees of freedom between them [25,26]. Special transition elements are necessary in order to combine the thin-shell elements having three displacement and two rotational degrees of freedom with the solid elements containing three displacement degrees of freedom. In this paper, the mixed element is applied to solve the discontinuity of the degrees of freedom between the solid elements and the thin-shell elements.

The internal tissues are discretized into a number of solid elements in the form of tetrahedrons, as shown in Fig. 2. The element displacements are defined by the 12 displacement components of the nodes as $U^e = [U_1 \quad U_2 \quad U_3 \quad U_4]^T$ with $U_i = [\bar{u}_i \quad \bar{v}_i \quad \bar{w}_i]^T, i = 1, 2, 3, 4$ (see Fig. 3a). The skin tissues are discretized into a number of thin-shell elements in the form of triangles, as shown in Fig. 2. A shell element is assembled by an in-plane (plane stress) element and a plate bending element. For the in-plane action, the state of strain is uniquely described in terms of the $\bar{u}_i$ and $\bar{v}_i$ displacement of each typical node, as shown in Fig. 3b. Similarly, for the bending action, the state of strain is given uniquely by the nodal displacement w in the z direction and the two rotations $\theta_{\bar{x}_i}$ and $\theta_{\bar{y}_i}$, as shown in Fig. 3c.

In order to transform the co-ordinate system from a local Cartesian co-ordinate system on the mid-surface of the element to a global co-ordinate system, $\theta_{\bar{z}_i} = 0$ is added to the displacement vectors of the shell element. Thus, the combined nodal displacement is defined below as $\bar{a}_i = [\bar{u}_i, \bar{v}_i, \bar{w}_i, \theta_{\bar{x}_i}, \theta_{\bar{y}_i}, \theta_{\bar{z}_i}]$ (see Fig. 3).

For a thin-shell element in the mixed elements, the stiffness matrix of the thin-shell element is made up of the two sub-matrices and defined as:

$$ {}^e\bar{\mathbf{K}}_{rs} = \begin{bmatrix} {}^e\bar{\mathbf{K}}^p_{rs} & & \\ & {}^e\bar{\mathbf{K}}^b_{rs} & \\ & & 0 \end{bmatrix} \tag{4} $$

where ${}^e\bar{\mathbf{K}}^p_{rs} = \begin{bmatrix} x^p & \\ & y^p \end{bmatrix}$ is the displacement sub-matrix in the x and y direction. ${}^e\bar{\mathbf{K}}^b_{rs} = \begin{bmatrix} z^p & & \\ & \theta^p_x & \\ & & \theta^b_y \end{bmatrix}$ is the sub-matrix including a displacement in the z direction and two rotations on the x and y axis. For a solid element in the mixed elements, the stiffness matrix is made up of the two sub-matrices and defined as:

$$ {}^e\mathbf{K}_{rs} = \begin{bmatrix} {}^e\mathbf{K}^{D_1}_{rs} & & \\ & {}^e\mathbf{K}^{D_2}_{rs} & \\ & & 0 \end{bmatrix} \tag{5} $$

where ${}^e\mathbf{K}^{D_1}_{rs} = \begin{bmatrix} x^{D_1} & \\ & y^{D_1} \end{bmatrix}$ is the displacement sub-matrix in the x and y direction. ${}^e\mathbf{K}^{D_2}_{rs} = \begin{bmatrix} z^{D_2} & & \\ & 0 & \\ & & 0 \end{bmatrix}$ is the sub-matrix including a displacement in the z direction and two rotations on the x and y axis.

Hence, a mixed element stiffness matrix is given by

$$ {}^e\mathbf{K}'_{rs} = \begin{bmatrix} {}^e\bar{\mathbf{K}}^p_{rs} + {}^e\mathbf{K}^{D_1}_{rs} & & \\ & {}^e\bar{\mathbf{K}}^b_{rs} + {}^e\mathbf{K}^{D_2}_{rs} & \\ & & 0 \end{bmatrix} \tag{6} $$

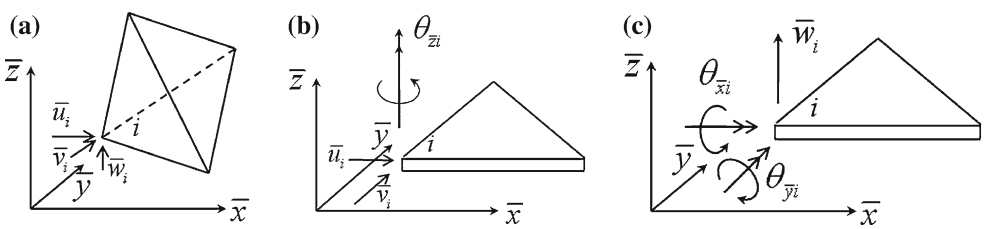

Fig. 3 **a** a tetrahedral solid element with three degrees of freedom each node, **b** a plane stress element including a rotation on the z axis and two displacements in the x and y directions, **c** a plate bending element including a displacement in the z direction and two rotations on the x and y axis

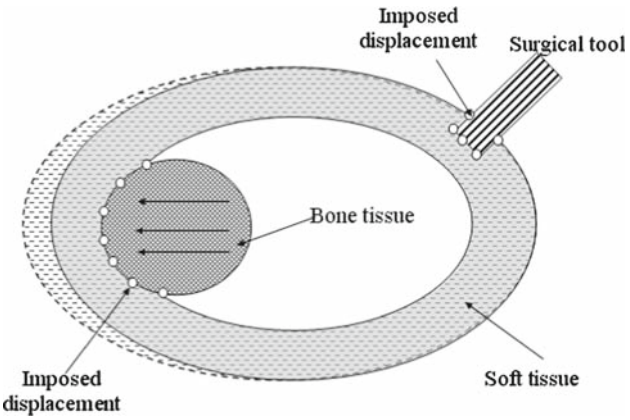

Fig. 4 The boundary conditions resulting from interaction with neighboring structures or with surgical tools

Boundary condition computation

In the surgical simulation, to assemble and resolve the finite element model described above, the bone-related boundary conditions have to be computed. The boundary conditions of a soft tissue model are related to the contacts with either bone tissues or surgical tools. The contacts between the bones (or the surgical tools) and the soft tissues may be posed, in theory, either as the imposed displacements or as prescribed the forces (see Fig. 4). Therefore, in the soft tissue simulation, the boundary condition computation of the finite element model means the detection of the contact vertices and the calculation of the imposed displacements of the contact vertices. Thus the main problem is to devise a stable contact algorithm to obtain the complex contact regions and the imposed displacements of the contact vertices. In this method, an improved contact model based on Hirota's contact model [27,28] is proposed. In this approach, a new distance field algorithm is employed to compute the penetration depth and normals.

Distance field computation

To compute the distance field of the geometric model, it is necessary to extract and initialize all vertices on the surface as zero distance nodes, followed by the calculation of distance values for each internal node in the geometric model. This algorithm to compute an internal distance field for geometrical model can be summarized as follows:

1) For each triangle of the surface, a prism is calculated by moving its vertices along the vertex normal by an amount of ζ in negative direction (ζ is the thickness of the distance envelope, and the value of ζ must depend on the application requirement).
2) For each prism of 1), the axis-aligned bounding box (AABB) enclosing the prism is determined.

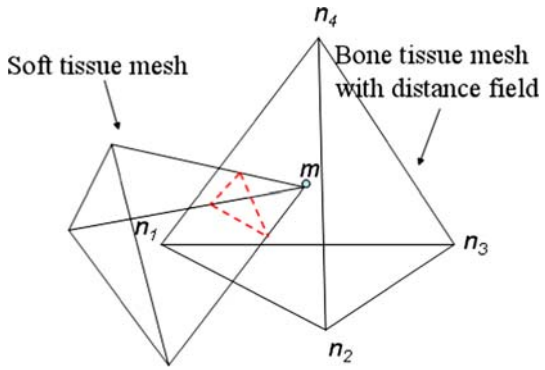

Fig. 5 Node m penetrates into another tetrahedral element, and the penetration depth is the distance of m to the face S_{124}

3) For all nodes of volumetric model that lie in the bounding box, the distance to the triangle of surface is computed.

Algorithm 1 shows the work-flow of distance field computation.

Algorithm 1 Distance field computation

Require: triangles $\sum$ of the surface with vertices normal $\mathbf{n}_i$, and N nodes of the geometric model
Output:distance field ψ
Initialization:$\psi \leftarrow +\infty$
for all triangles $t \in \sum$ **do**
  $P \leftarrow$ComputePrism($t, \mathbf{n}_1, \mathbf{n}_2, \mathbf{n}_3, \zeta$)
  $B \leftarrow$ComputeAABB(P)
  $V \leftarrow$ComputeNodesInAABB(B,N)
  for all $p \in V$ **do**
    $d \leftarrow$ComputeMinimumDistance(p,t)
    $\psi(p) \leftarrow$min(d, $\psi(p)$)
  end for
end for

Imposed displacement computation

An interpolation method is proposed to calculate the imposed displacements of the contact vertices. As shown in Fig. 5, one of the contact vertices of the soft tissue model penetrates the bone model. The following equation is used to compute the imposed displacement:

$$d = u_1 d_1 + u_2 d_2 + u_3 d_3 + (1 - u_1 - u_2 - u_3) d_4 \qquad (7)$$

where d_1, d_2, d_3 and d_4 are distance values at the four nodes of each tetrahedral element. These distance values are obtained directly from the distance field generated by "Distance field computation". The interpolation parameters, u_1, u_2 and u_3, are derived from the interpolation functions of the element, and $0 \leq u_i \leq 1, 1 \leq i \leq 3$. The value of d is quickly computed at any point inside the object. Suppose a boundary node $\mathbf{m}$ is within an element with nodes $\mathbf{n}_1$, $\mathbf{n}_2$, $\mathbf{n}_3$ and

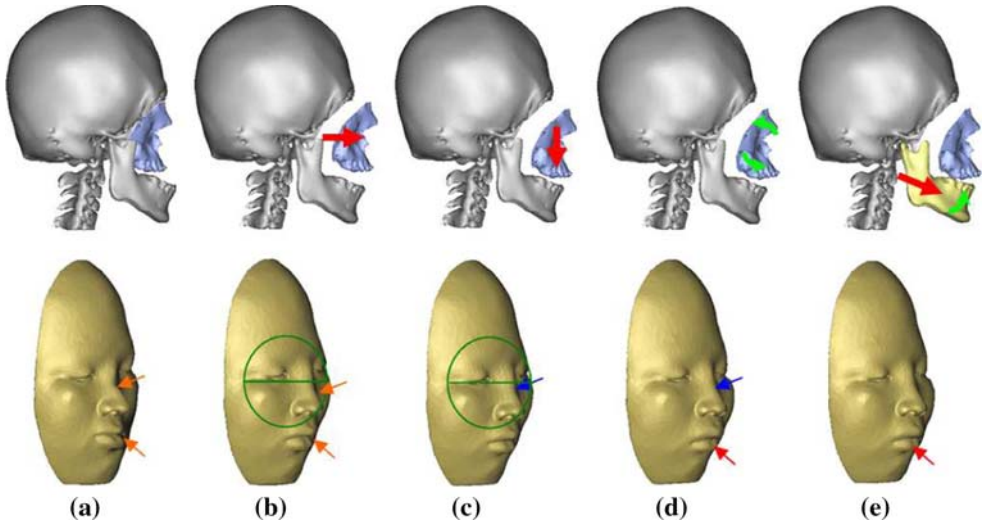

Fig. 6 Results of soft tissue deformation based on bone-related planning, **a** bone cuts and pre-operative face, **b** mid-face moving 12 mm forwards and the corresponding soft tissue deformation, **c** mid-face moving 5 downwards and the corresponding result, **d** mid-face rotating 5° anti-clockwise and the result, **e** mandible moving 8 mm forward and rotating 3° anti-clockwise and the result

$\mathbf{n}_4$ as shown in Fig. 5. m can be written in terms of linear interpolation of $n_1, \ldots, n_4$:

$$\mathbf{m} = u_1\mathbf{n}_1 + u_2\mathbf{n}_2 + u_3\mathbf{n}_3 + (1 - u_1 - u_2 - u_3)\mathbf{n}_4 \tag{8}$$

d at $\mathbf{m}$ is obtained by solving Eqs. 1 and 2

$$d = [d_1 - d_4, d_2 - d_4, d_3 - d_4]\,\mathbf{G}^{-1}\,[\mathbf{m} - \mathbf{n}_4] + d_4 \tag{9}$$

where $\mathbf{G} = [\mathbf{n}_1 - \mathbf{n}_4, \mathbf{n}_2 - \mathbf{n}_4, \mathbf{n}_3 - \mathbf{n}_4]$

Contact force

We assume that the contact between the bones and the soft tissues is frictionless, and thus the contact force is normal to the surface. The normal is the partial derivative of a gap function g with respect to spatial coordinates. Thus the contact force is

$$\mathbf{f}_c = p_c\mathbf{n} = p_c\frac{\partial g(\mathbf{x})}{\partial \mathbf{x}} \tag{10}$$

where p_c is contact pressure which can be replaced with penalty $k_c g$ as

$$\mathbf{f}_c = k_c g(\mathbf{x})\frac{\partial g(\mathbf{x})}{\partial \mathbf{x}} \tag{11}$$

where k_c is a penalty constant.

Note that the contact force is the partial derivative of penalty-potential energy $\phi = k_p g^2/2$, namely

$$\frac{\partial \phi}{\partial \mathbf{x}} = \frac{\partial}{\partial \mathbf{x}}\left(\frac{1}{2}k_c g^2\right) = k_c g(\mathbf{x})\frac{\partial g(\mathbf{x})}{\partial \mathbf{x}} \tag{12}$$

In the paper, the penalty-potential energy is defined as a function of imposed displacements

$$\phi(d) = k_c d^2 \tag{13}$$

The external contact force is therefore computed as follows:

$$\mathbf{F}_a^{\text{ext}} = \int_{\partial V^{(c)}} \frac{\partial \phi}{\partial \mathbf{x}} N_a \mathrm{d}a \tag{14}$$

Results

Implementation procedure

To explain the system implementation, a case of craniofacial dysostosis is used in the paper, whose objective is to simulate correction of craniofacial dysostosis with distraction osteotogenesis. Figure 6 shows the bone movements with different bone-related planning and the corresponding results of the deformation of the soft tissues.All calculations were performed on a workstation with a Dual-Core AMD Opteron CPU 3.0GHz, with 4G of RAM and a NVIDIA Quadro FX 5500 GPU. The implementation workflow consists of the following steps:

(1) Geometric modeling and pre-processing: To create the 3D geometric models, including the bone tissue models and the soft tissue models, it is necessary to reconstruct and optimize surface meshes of the face tissues from CT data sets. The external surface of the internal tissues and the mid-face of the thin-shell element are

Table 2 The data sets of 6 patients

Procedure	BC computation time (s)	Imposed vertices	Error vertices	Error ratio(%)
(1)	0.468	3258	33	1.01
(2)	0.538	3657	56	1.53

obtained following the method described in "Mixed element modeling". Thus, the thin-shell elements are first generated. Then, the tetrahedral models for the internal soft tissues and the bones are built with the finite element analysis tools(ABAQUS 6.5). During the pre-processing, the 3D distance field of the bone geometric models can be calculated using our algorithm described Section "Distance field computation". In this simulation, the thickness of the distance field is assumed as 3 mm since the moving of the bones in each step is less than 3 mm so as to reduce the collision detection error.

(2) Osteotomies: The bone cuts (osteotomies) are modeled with the help of a craniofacial surgeon. The required cut surfaces for defining the bone regions are interactively generated following the anatomy structures,as shown in Fig. 6a.

(3) Boundary conditions: Following the bone movements, we first need to detect the contact regions between the moved bones and the soft tissues using a collision detection algorithm [29]. Subsequently, the imposed displacements on the soft tissue model are calculated following the bone movements. There are two types of displacements on the soft tissue model: zero displacements (fixed nodes) and nonzero imposed displace ments. Nonzero imposed displacements can be estimated using the distance field and the interpolation algorithm described in "Imposed displacement computation". Next, we can turn to the previous step if the bones need to be moved again.

(4) Simulation: The geometrical model built on the mixed elements and the boundary conditions serve as input for our simulator. We used the improved biomechanical model described in "Method" to model the facial soft tissue behavior and to predict the new facial outline.

Validation

Boundary conditions

In order to apply the biomechanical model to the soft tissue simulation, it is necessary to have an efficient and accurate contact algorithm to compute the external contact forces between the bones and the soft tissues in the surgical planning system. For the soft tissue model of the face, it is very difficult to estimate the contact force using such conventional methods as manual editing, registration and so on due to the complexity of the facial geometric structures. Therefore, the computational strategy of the boundary conditions presented in this paper has great significance to promote the development of the soft tissue prediction systems based on bone-related planning. It not only helps us estimate the contact forces between the bones and the soft tissues automatically, but also improves the accuracy and the efficiency of the surgical planning system. However, in the previous work of the surgical simulation, few researchers proposed and used this kind of method. The effectiveness and accuracy of this method are thus demonstrated in this paper.

We have chosen two typical parts of the head, including the mandible and the mid-face, to validate the accuracy of boundary condition computation. Table 2 shows the statistic results of the boundary condition computation. The average error ratio stays below 2%. Compared to previous methods, the accuracy of the boundary condition computation has been greatly improved. In addition, we evaluate the computation time of the boundary conditions at each step. As shown in Table 2, although the number of the contact vertices is large, the computation time in these experiments is less than 1 s. Compared to the finite element modeling computation, the running speed is fast enough for the soft tissue deformation.

Simulation of soft tissue deformation

The way to truly measure the accuracy of the prediction is by comparing post-operative data with the predicted data [1,30]. For these measurements, the predicted and post-operative facial skin surfaces are first rigidly registered based on an unaltered sub-volume and subsequently the distance between both surfaces is determined. The distance map is computed using a signed Euclidean distance [30].

The 6 patients' data sets were processed as described above. To improve the validation, the eye regions of each patient were manually selected and omitted during processing. Differences in these regions are mainly due to opening or closing of the eyelids during acquisition of the pre-operative and post-operative CT scan. Figure 7 shows the distance maps for each of the 6 patients. The color map ranges between −3 and 3 mm, where a negative error means that the predicted skin surface lies behind the post-operative skin surface. We found that some typical regions(the lips and the nose) with large errors.

In addition, we selected a patient data set and compared the results of the four different computational strategies. They

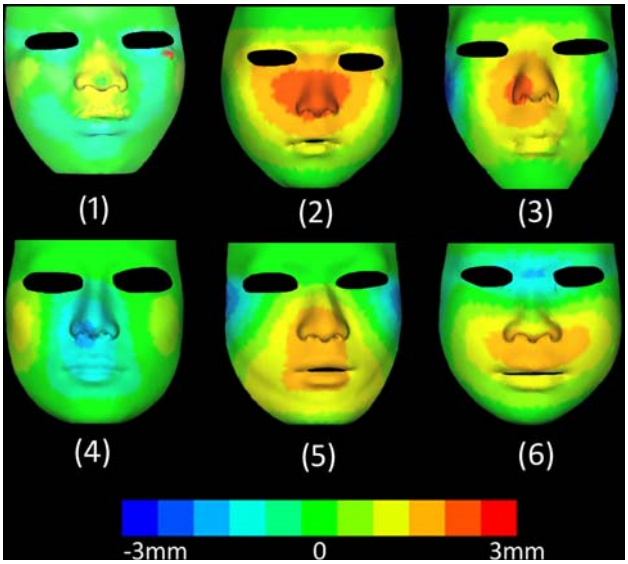

Fig. 7 Distance maps visualized by color coding for the 6 patients

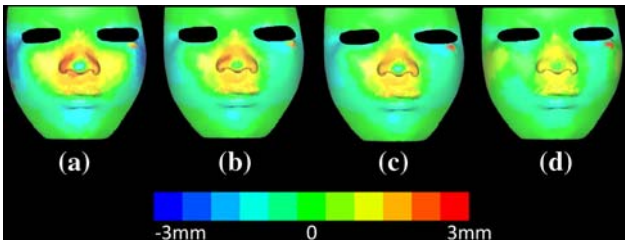

Fig. 8 Comparison of the four different computational models for the same patient

are linear finite element modeling (LFEM), mass tensor modeling (MTM), nonlinear finite element modeling (NFEM) and nonlinear Finite Mixed Element Modeling (NFM-EM). In the FEM, MTM and NFEM, the soft tissues are modeled with uniform tetrahedral meshes, and the interpolation between the mesh nodes are implemented by using a basic linear, C_0 continuous shape function for each tetrahedron. As shown in Fig. 8, the outcome of the statistical analysis for all four computational models shows that the most accurate result is obtained with NFM-EM. The average absolute value of errors is 0.5 mm and the 95% percentiles of the distance map is less than 1.5 mm. The linear FEM is frequently used to predict the small deformation of soft tissues but here it lacks sufficient accuracy(only 79% percentiles of the region is less than 1.5 mm) due to the large deformation. The MTM and the NFEM do not have this drawback but do not incorporate tissue specific behavior so that they only have 87 and 89% percentiles, respectively.

Discussion

The proposed method is successfully demonstrated in a preliminary application to complex cranio-maxillofacial surgery. The implementation develops a new biomechanical model based on mixed-elements that not only maintains the features of the finite volumetric element method, but also provides C_1 continuous finite element surfaces. As a result, the soft tissues of the face were discretized into solid elements with tetrahedrons and thin-shell elements with triangular meshes. In this way, the different biomechanical characteristics of the skin and internal tissues were effectively incorporated into the soft tissue model of the face, enabling the potential for significantly higher accuracy in soft tissue simulation.

The estimate of the material parameters of the facial soft tissues is a key step in the biomechanical analysis. We investigated the different hyper-elastic strain potential functions, including Mooney–Rivlin form, Ogden form and Polynomial form, and found out the Mooney–Rivlin form is the best model to approximate the stress–strain relationship of the skin, muscles and fat. In this paper, therefore, we selected the Mooney–Rivlin model to be the strain potential function.

The boundary condition computation is another key step in the biomechanical analysis. The nonlinear finite element modeling is more sensitive to the boundary conditions and material parameters of the model, which results in the NFEM cannot improve the simulation accuracy in previous research works. In this paper, a fast and robust contact algorithm was used to estimate dynamically the boundary conditions and addresses the problem of the boundary conditions of the NFM-EM, which ensures the convergence of the NFM-EM and the precision of the solution.

For the quantitative validation, the statistic analysis results show that the average error stays below 0.5 mm for each patient and the 95% percentiles is less than 1.5 mm. Furthermore, for the four different computational strategies, consisting of the LFEM, MTM, NFEM and NFM-EM, the NFM-EM has the highest quality and accuracy. Although there are typical regions (the nose and lips) with large errors due to an expression change in these regions during acquisition of the pre-operative and post-operative CT scan, the surgeons are satisfied with the accuracy of the NFM-EM. However, when we asked some plastic surgeons from Shanghai 9th People Hospital for helping us validate this simulator. They thought this simulator can provide relatively accurate results for the prediction of craniofacial surgery, but they have to do much interaction work and must spend much time on using our simulator since during the simulation they first must reconstruct the special geometric model of the soft tissues using manual segmentation and reconstruction method, and define the cut regions with the manual measurement method depending on surgeons' experience. Second, in each step, it takes much

computational time to compute the biomechanical model. Therefore, they also expect the simulator described in the paper to be applied in the CSPS with less intervention and less computational time.

Conclusion

It is highly desirable to develop an accurate surgical planning system which can arrange the bone-related planning and predict the target face. In this paper, an improved nonlinear finite element modeling is proposed to improve the accuracy of soft tissue deformation, and an effective contact algorithm can bridge the bone-related planning and the prediction of the target face.

The quantitative validation shows that the NFM-EM is effective and accurate for several complex craniofacial surgery simulation. The average error stays below 0.5 mm for each patient and the 95% percentiles is less than 1.5 mm. The efficient contact algorithm makes it easy to implement the deformation simulation of the soft tissues after movements and rotations of the bones. Therefore, this approach can be widely applied in surgery simulation, even complex craniofacial surgery.

For future work, we will improve our method even more. First, the material properties of the living tissues will be further investigated. Second, in order to decrease the intervention, we consider automated ways for defining the cut regions based on facial anatomy and desired post-operative facial appearances. Finally, much more qualitative and quantitative validation is required for further studies. For the quantitative validation, we can compare the predicted results with the post-operative results using much more clinical cases, and for qualitative validation,we can use the qualitative protocols[1,18] to prove the effectiveness of the results.

Acknowledgments The authors would like to thank the anonymous reviewers and editors for their comments and suggestions, which helped improve the quality of this work greatly. The research was supported by Shanghai Leading Academic Discipline Project (Project Number: S30602) and Shanghai Science Foundation of China (No. 08ZR 1409300). The authors would like to thank Prof. Xiongzheng Mu and Dr. Zheyuan Yu in the Shanghai 9th People's Hospital for their assistance in acquiring patients' data set and validating the results.

References

1. Mollemans W, Schutyser F, Nadjmi N et al (2007) Predicting soft tissue deformations for a maxillofacial surgery planning system: from computational strategies to a complete clinical validation. Med Image Anal 1:282–301
2. Terzopoulos D, Walters K (1990) Physically-based facial modelling, analysis and animation. Vis Comput Anim 1(4):73–80
3. Lee Y, Terzopoulos D, Walters K (1995) Realistic modeling for facial animation. Comput Graphics (Ann Conf Ser) 29:55–62
4. Koch RM, Gross MH, Carls FR et al (1996) Simulating facial surgery using finite element models. In: Proceedings of SIGGRAPH 96. ACM press, New Orleans, pp 421–428
5. Keeve E, Girod S, Pfeifle P et al (1996) Anatomy-based facial tissue modeling using the finite element method. In: Proceedings of IEEE Visualization'96. IEEE Computer Society, San Francisco, pp 21–28
6. Bro-Nielsen M, Cotin S (1996) Real-time volumetric deformable models for surgery simulation using finite elements and condensation. Comput Graphics Forum 15(3):57–77
7. Cotin S, Delingette H, Ayache N (1999) Real-time elastic deformations of soft tissues for surgery simulation. IEEE Trans Vis Comput Graphics 5(1):62–73
8. Cotin S, Delingette H, Ayache N (2000) A hybrid elastic model allowing real-time cutting, deformations and force-feedback for surgery training and simulation. Vis Comput 16(8):437–452
9. Zhuang Y, Canny J (2000) Haptic interactions with global deformations. In: IEEE International conference on robotics and automation, San Francisco, USA, pp 2428–2433
10. Delingette H (1998) Toward realistic soft-tissue modeling in medical simulation. In: Proceedings of IEEE special issue on surgery simulation. IEEE Computer Society, San Francisco, pp 512–523
11. Wu X, Downes M, Goktekin T, Tendick F (2001) Adaptive nonlinear finite elements for deformable body simulation using dynamic progressive meshes. In: Proceedings of Eurographics 2001, Manchester, UK, pp 349–358
12. Picinbono G, Delingette H, Ayache N (2001) Non-linear and anisotropic elastic soft tissue models for medical simulation. In: IEEE international conference on robotics and automation, vol 2, Seoul, Korea. pp 1370–1375
13. Picinbono G, Delingette H, Ayache N (2003) Non-linear anisotropic elasticity for real-time surgery simulation. Graph Models 65(5):305–321
14. Gladilin E, Zachow S, Deuflhard P, Hege HC (2001) A biomechanical model for soft tissue simulation in craniofacial surgery. In: Proceedings of MIAR. pp 137–141
15. Schwartz JM, Deniger M, Rancourt D et al (2005) Modeling liver tissue properties using a non-linear visco-elastic model for surgery simulation. Med Image Anal 2:103–112
16. Sokhanvar SJD, Packirisamy M (2008) Hyperelastic modelling and parametric study of soft tissue embedded lump for mis applications. Int J Med Robot Comput Assist Surg 4(3):232–241
17. Chabanas M, Luboz V, Payan Y (2003) Patient specific finite element model of the face soft tissues for computer-assisted maxillofacial surgery. Med Image Anal 7:131–151
18. Westermark A, Zachow S, Eppley B (2005) Three-dimensional osteotomy planning in maxillofacial surgery including soft tissue prediction. J Craniofac Surg 16(1):100–104
19. Mooney M (1940) A theory of large elastic deformation. J Appl Phys 11:582–592
20. Fung Y (1993) Biomechanics: mechanical properties of living tissue. Springer, New York
21. Kvistedal YA, Nielsen PMF (2004) Investigating stress-strain properties of in-vivo human skin using multiaxial. In: Proceedings of the 26th IEEE EMBS. IEEE Computer Society, San Francisco, pp 5096–5099
22. Lorensen WE, Cline HE (1987) Marching cubes: a high resolution 3d surface construction algorithm. Comput Graphic 21(4):163–169
23. Keeve E, Schaller S, Girod S, Girod B (1997) Adaptive surface data compression. Special Issue Signal Process Med Image Compress 59(2):211–220
24. Paiva A, Lopes H, Lewiner T (2006) Robust adaptive meshes for implicit surfaces. In: IEEE proceedings of the XIX Brazilian symposium on computer graphics and image processing (SIBGRAPI'06), pp 205–212

25. Hauptmann R, Schweizerhof K (1998) A systematic development of 'solid-shell' element formulations for linear and non-linear analyses employing only displacement degrees of freedom. Int J Numer Methods Eng 42:49–69
26. El-Abbasi N, Bathe KJ (2001) Stability and patch test performance of contact discretizations and a new solution algorithm. Comput Struct 29:1473–1486
27. Hirota G, Fisher S, State A, Lee FH C (2001) An implicit finite element method for elastic solids in contact. In: Proceedings of the 14th IEEE conference on computer animation. pp 136–146
28. Hirota G, Fisher S, State A (2003) An improved finite-element contact model for anatomical simulations. Vis Comput 19:291–309
29. Maciel A, Boulic R, Thalmann D (2007) Efficient collision detection within deforming spherical sliding contact. IEEE Trans Vis Comput Graphics 13(3):518–529
30. Chabanas M, Payan Y, Marecaux C et al (2004) Comparison of linear and non-linear soft tissue models with post-operative ct scan in maxillofacial surgery. Lecture Notes in computer science. Springer, Heidelberg, pp 19–27